Article

Structure

The Human Centriolar Protein CEP135 Contains a Two-Stranded Coiled-Coil Domain Critical for Microtubule Binding

Highlights

- The N terminus of HsCEP135 (HsCEP135-N) forms a coiled-coil structure
- HsCEP135-N binds tubulin, protofilaments, and microtubules
- HsCEP135-N segment 96–108 is a major microtubule-binding site
- HsCEP135-N could contribute to the formation of centriolar microtubule triplets

Authors

Sebastian Kraatz, Paul Guichard, Jagan M. Obbineni, ..., John Missimer, Pierre Gönczy, Michel O. Steinmetz

Correspondence

michel.steinmetz@psi.ch

In Brief

Kraatz et al. show that the N-terminal domain of human CEP135/Bld10p (HsCEP135-N) forms a coiled-coil structure that binds tubulin, protofilaments, and microtubules. The authors further found that segment 96–108 of HsCEP135-N is a major microtubule-binding site. Their results have implications for centriolar microtubule triplet formation.

Accession Numbers

5FCN
5FCM

Kraatz et al., 2016, Structure *24*, 1358–1371
August 2, 2016 © 2016 Elsevier Ltd.
http://dx.doi.org/10.1016/j.str.2016.06.011

CellPress

CellPress

Structure
Article

The Human Centriolar Protein CEP135 Contains a Two-Stranded Coiled-Coil Domain Critical for Microtubule Binding

Sebastian Kraatz,[1] Paul Guichard,[2,3] Jagan M. Obbineni,[1] Natacha Olieric,[1] Georgios N. Hatzopoulos,[2] Manuel Hilbert,[1] Indrani Sen,[1] John Missimer,[1] Pierre Gönczy,[2] and Michel O. Steinmetz[1,*]

[1]Laboratory of Biomolecular Research, Department of Biology and Chemistry, Paul Scherrer Institut, 5232 Villigen, Switzerland

[2]Swiss Institute for Experimental Cancer Research (ISREC), School of Life Sciences, Swiss Federal Institute of Technology (EPFL), 1015 Lausanne, Switzerland

[3]Present address: Department of Cell Biology, Sciences III, University of Geneva, 1211 Geneva, Switzerland

*Correspondence: michel.steinmetz@psi.ch

http://dx.doi.org/10.1016/j.str.2016.06.011

SUMMARY

Centrioles are microtubule-based structures that play important roles notably in cell division and cilium biogenesis. CEP135/Bld10p family members are evolutionarily conserved microtubule-binding proteins important for centriole formation. Here, we analyzed in detail the microtubule-binding activity of human CEP135 (HsCEP135). X-ray crystallography and small-angle X-ray scattering in combination with molecular modeling revealed that the 158 N-terminal residues of HsCEP135 (HsCEP135-N) form a parallel two-stranded coiled-coil structure. Biochemical, cryo-electron, and fluorescence microscopy analyses revealed that in vitro HsCEP135-N interacts with tubulin, protofilaments, and microtubules and induces the formation of microtubule bundles. We further identified a 13 amino acid segment spanning residues 96–108, which represents a major microtubule-binding site in HsCEP135-N. Within this segment, we identified a cluster of three lysine residues that contribute to the microtubule bundling activity of HsCEP135-N. Our results provide the first structural information on CEP135/Bld10p proteins and offer insights into their microtubule-binding mechanism.

INTRODUCTION

The centriole and the related basal body are organelles that are essential for the formation of the centrosome, the major microtubule organizing center in animal cells, as well as of the axoneme in cilia and flagella (reviewed in Bornens, 2012). Due to their functional importance, alterations in centriole structure or function are linked to severe human diseases, including several forms of ciliopathy and cancer (reviewed in Bettencourt-Dias and Hildebrandt, 2011; Nigg and Raff, 2009). Centrioles are typically constructed around a 9-fold symmetric "cartwheel" structure consisting of a central hub from which nine spokes emanate. An electron-dense region called the "pinhead" connects each of these spokes to a microtubule multiplet, which collectively form the microtubule wall of the centriole (Guichard et al., 2013). Despite important progress in recent years, the mechanisms that govern formation of the remarkable and evolutionarily conserved architecture of centrioles remain elusive, owing in part to a paucity of structural information of participating components.

Several players important for promoting centriole assembly and stability have been identified over the last decade in different organisms (reviewed in Azimzadeh and Marshall, 2010; Gönczy, 2012; Hirono, 2014). Among them, the essential cartwheel protein SAS-6 was one of the first to have been studied in great detail; structural and biophysical data revealed that the self-assembly properties of SAS-6 proteins establish the central hub and a large part of the spokes of the cartwheel and are thus key in determining the 9-fold symmetry of centrioles (Van Breugel et al., 2011; Kitagawa et al., 2011). Another evolutionarily conserved and important centriolar protein is CEP135/Bld10p (Ohta et al., 2002; Ryu et al., 2000), which plays a critical role for proper centriole formation in *Chlamydomonas reinhardtii*, *Paramecium tetraurelia*, and *Tetrahymena thermophilia*. Depletion phenotypes in these unicellular organisms range from a complete loss of centrioles in *Chlamydomonas* to defects in centriole assembly and SAS-6 maintenance in *Paramecium* or loss of centriolar microtubules in *Tetrahymena* (Bayless et al., 2012; Hiraki et al., 2007; Jerka-Dziadosz et al., 2010; Matsuura et al., 2004). In *Drosophila melanogaster*, CEP135/Bld10p depletion leads to shortened centrioles and to an increase in centriole diameter (Mottier-pavie and Megraw, 2009; Roque et al., 2012). Furthermore, *Drosophila* CEP135/Bld10p is critical for assembly of the central microtubule pair of the sperm axoneme (Carvalho-Santos et al., 2012) and plays an important role for asymmetric cell division of neuroblasts (Singh et al., 2014). In the case of chordates, the reported CEP135/Bld10p depletion phenotypes vary somewhat. In DT40 chicken cells, for example, only weak alterations in centriole numbers were observed on CEP135/Bld10p gene disruption (Lalor et al., 2013). By contrast, primary fibroblasts derived from patients suffering from microcephaly due to a premature termination codon in the human CEP135/Bld10p gene display aberrations in centrosome numbers (Hussain et al., 2012). Furthermore, small interfering RNA-mediated

CrossMark

depletion of CEP135/Bld10p in human cultured cells causes a loss of centriolar microtubules, as well as a reduction in centriole length (Lin et al., 2013; Dahl et al., 2015), reminiscent of the phenotype obtained in *Drosophila*. Together, these observations suggest that CEP135/Bld10p plays an important role in promoting centriole assembly and stability, although its exact mode of action appears to differ somewhat depending on the species.

Immunofluorescence and electron microscopy (EM) studies ascertained that human CEP135/Bld10p localizes principally to the proximal lumen of the parental centriole and to a lesser extent to the lumen of the growing procentriole (Kleylein-Sohn et al., 2007; Sonnen et al., 2012). On the other hand, work in *Chlamydomonas* and *Paramecium* revealed the presence of CEP135/Bld10p at the cartwheel-microtubule connection in the proximal part of centrioles (Hiraki et al., 2007; Jerka-Dziadosz et al., 2010; Matsuura et al., 2004). Interestingly, a microtubule-binding site has been mapped to the N-terminal part of human (segment 1–190) and *Drosophila* (segment 1–163) CEP135/Bld10p (Carvalho-Santos et al., 2012; Lin et al., 2013). Collectively, these studies suggest that CEP135/Bld10p proteins stabilize centrioles by interacting with their cartwheels and/or with their microtubule walls.

In this study we sought to investigate in detail the microtubule-binding site of human CEP135/Bld10p (denoted HsCEP135 from here onwards). Based on X-ray crystallography, small-angle X-ray scattering (SAXS), and molecular modeling, we produced an atomic model for the N-terminal domain of HsCEP135 (HsCEP135-N). We further defined a major microtubule-binding site in this domain using biochemical, cryo-EM, and fluorescence microscopy experiments and pinpointed by rational mutagenesis three lysine residues that contribute to the microtubule bundling activity of HsCEP135-N. Our results represent the first high-resolution structural information on a CEP135/Bld10p family member and provide insights into how HsCEP135 interacts with microtubules.

RESULTS AND DISCUSSION

Biophysical and Functional Characterization of the N-Terminal Domain of HsCEP135

Bioinformatic analyses suggested that HsCEP135 is extensively helical and contains several long regions that are predicted to form coiled-coil structures (Figure 1A) (Carvalho-Santos et al., 2010; Matsuura et al., 2004). A multiple sequence alignment of CEP135 orthologs revealed an ~160 N-terminal sequence stretch that coincides with a predicted structured region (Carvalho-Santos et al., 2010). In human and fly proteins, this region of CEP135 has been shown to contain a microtubule-binding site (Carvalho-Santos et al., 2012; Lin et al., 2013). Overall, these observations suggest that the first ~160 N-terminal residues of CEP135 family members form an evolutionarily conserved functional domain that binds microtubules.

To biophysically characterize the N-terminal domain of HsCEP135, we recombinantly expressed and purified the first 158 residues of the protein (denoted HsCEP135-N; Figure 1A). The secondary structure and thermal stability of HsCEP135-N in solution was assessed by circular dichroism (CD) spectroscopy. As shown in Figure 1B, the far-UV CD spectrum from HsCEP135-N recorded at 4°C was typical for an α-helical coiled-coil structure exhibiting minima at 208 and 222 nm and a $[\Theta]_{222}$:$[\Theta]_{208}$ ratio of >1 (Zhou et al., 1992). Thermal unfolding experiments recorded by CD at 222 nm and at an HsCEP135-N concentration of 10 μM revealed a sigmoidal-shaped profile characteristic of a cooperatively folded protein with a midpoint of the transition, T_m, centered at 56°C (Figure 1C; Table 1). The oligomerization state of HsCEP135-N was assessed by size-exclusion chromatography followed by multi-angle light scattering (SEC-MALS). A molecular mass of 42 kDa was obtained, consistent with the formation of a homodimer (calculated molecular mass of the monomer: 18.7 kDa; Figure 1D; Table 1).

The microtubule-binding activity of HsCEP135-N was tested by a standard microtubule pelleting assay (Campbell and Slep, 2011). As shown in Figure 1E, while HsCEP135-N did not pellet on its own, it did so in the presence of microtubules, consistent with previous results (Lin et al., 2013). Inspection by cryo-EM of microtubules incubated with HsCEP135-N revealed that the protein decorated microtubules (Figures 2A and 2B), indicating that the interaction between CEP135-N and microtubules is specific. Cryo-tomographic reconstructions of such samples suggested that the decoration most likely reflected the presence of protofilament-based rings and/or spirals that wrap around the microtubule shaft (Figures S1A and S1B). Consistent with this hypothesis, analysis of tomograms revealed a pronounced density with a periodicity of ~8 nm along the long axis of the microtubule, which matches the spacing between tubulin dimers (Figures 2C and 2D). We further observed that, besides decorating microtubules, HsCEP135-N can also induce the formation of protofilament-based ring-like structures in the presence of soluble tubulin (Figures S1C–S1E). Interestingly, when tubulin was co-polymerized together with HsCEP135-N, we observed microtubules that were occasionally bridged with either individual straight protofilaments (Figure 2E) or with other microtubules (Figures 2F and 2G).

Collectively, these results suggest that HsCEP135-N forms a very stable two-stranded coiled-coil structure. They further indicate that in vitro, HsCEP135-N binds directly to tubulin, protofilaments, and microtubules and has the capacity to bridge such higher-order assemblies. Protofilament-based ring-like oligomers either in isolation or wrapped around microtubules are frequently obtained in the presence of divalent cations or of isolated domains from microtubule-associated proteins (Tan et al., 2006; Wang et al., 2014) and are typically associated with a microtubule depolymerization activity (Mandelkow et al., 1991; Desai et al., 1999); however, we did not find any indication that HsCEP135-N destabilizes microtubules (Figures 2A and 2B, see also below). Whether these protofilament-based ring-like oligomers are also formed in the presence of the full-length HsCEP135 protein and whether they are of any functional relevance remains to be determined.

Structural Model of HsCEP135-N

To provide a structural basis for understanding the interaction of HsCEP135-N with microtubules, we analyzed its structure by X-ray crystallography and in solution by SAXS. Crystallization of HsCEP135-N and the corresponding domain from the *Chlamydomonas* ortholog CrBld10p were not successful. However, after extensive fragment screening, we solved the structures of

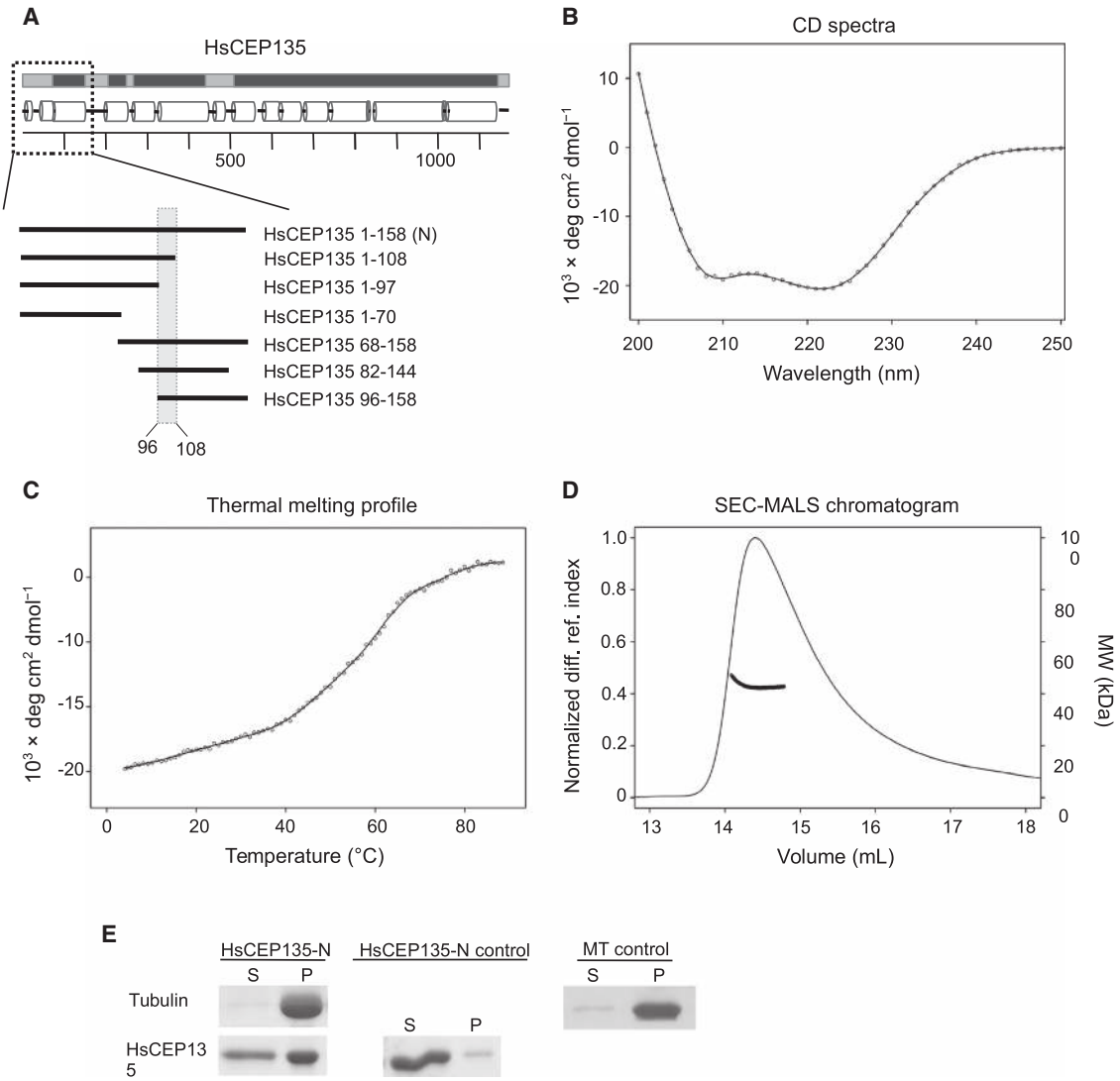

Figure 1. Characterization of HsCEP135-N

(A) Top: coiled-coil (black and gray bars) and secondary structure (white cylinders) prediction of HsCEP135. Black and gray boxes highlight regions with 80%–100% and <80% coiled-coil probability, respectively. White cylinders depict predicted α-helical regions. Bottom: schematic representation of protein fragments used in this study. The dashed box highlights the N-terminal domain of HsCEP135. The gray vertical bar highlights segment 96–108, which is crucial for microtubule binding of HsCEP135-N.

(B and C) Spectra (B) and thermal unfolding profile (C) recorded by CD from HsCEP135-N (10 μM). The spectra and the unfolding profile were obtained at 4°C and at 222 nm, respectively. See also Table 1. Symbols and the line in (C) represent data points and the spline fit to the data, respectively.

(D) SEC-MALS experiment obtained by injecting 100 μl of a 200 μM HsCEP135-N protein solution.

(E) Microtubule pelleting assay for HsCEP135-N and representative controls. Shown are relevant areas of Coomassie-stained SDS-PAGE gels corresponding to the proteins of interest. S, supernatant; P, pellet; MT, microtubule.

CrBld10p-N 1–70 and HsCEP135-N 82–144 to 2.2 and 1.8 Å resolution, respectively (Table 2).

As shown in Figure 3A, the crystal obtained with CrBld10p-N 1–70 revealed four monomers in the asymmetric unit, which are organized into two individual dimers. The ~20 N-terminal residues of each monomer form short α helices that assume different orientations, presumably as a result of crystal contacts (Figure S2A). Residues ~35–60 form a two-stranded parallel and in register coiled-coil structure, where hydrophobic heptad **a** and **d** core residues pack in a characteristic "knobs-into-holes" fashion (Walshaw and Woolfson, 2001). The N-terminal and coiled-coil helices are connected by a ~5–10 amino-acid-long linker region. The dimeric and cooperatively folded helical nature of CrBld10p-N 1–70 was confirmed by CD and SEC-MALS (Figures S4A and S4B; Table 1). To obtain structural information on the N-terminal residues of CrBld10p-N 1–70 in solution, we recorded SAXS data (Figure 4A). The calculated pair distribution function (representing a distribution function of inter atomic distances) revealed a distinct peak centered at 20 Å and a maximum particle distance, D_{max}, of 86 Å (Figures 4B and S3A; Table 3), in good agreement with the thickness (22 Å) and elongated nature of a two-stranded coiled-coil structure. Notably, the

Table 1. Biophysical Characterization and Microtubule-Binding Activity of CEP135/Bld10p Fragments

Protein	Construct	T_m[a] (°C)	Calculated MW[b] (kDa)	Determined MW[c] (kDa)	Oligomerization State	MT-Binding Activity[d]
HsCEP135	1–158	56	18.67	43	dimer	+
HsCEP135	1–70	58	8.24	14.2	dimer	–
HsCEP135	1–108	43	12.88	28.8	dimer	+
HsCEP135	1–97	42	11.59	22.4	dimer	–
HsCEP135	68–158	39	10.93	22	dimer	+
HsCEP135	96-158 r.	–	7.44	7.2	monomer	ND
HsCEP135	96-158 n.r.	57	7.44	12.2	dimer	+
HsCEP135	1-158 K101,104,108A	37	18.50	41.9	dimer	+/–
HsCEP135	1-108 K101,104,108A	42	12.71	24.7	dimer	+/–
HsCEP135	68-158 K101,104,108A	24	10.75	23.2	dimer	+/–
HsCEP135	96-158 K101,104,108A n.r.	44	7.27	14.5	dimer	–
CrBld10	1–70	30	7.95	14.2	dimer	–

MW, molecular weight; MT, microtubule; ND, not determined; r., experiment performed under reducing buffer conditions; n.r., experiment performed under non-reducing buffer conditions.
[a]Determined by far-UV CD.
[b]Based on primary amino acid sequence.
[c]Determined by SEC-MALS.
[d]Determined by MT-pelleting assays.

experimentally determined pair distribution function did not match any of the ones calculated from the homo-dimeric configurations modeled from the four monomer structures present in the asymmetric unit of the crystal (Figures 3A and 4B), suggesting that the ~30 N-terminal residues of CrBld10p-N 1–70 are indeed largely disordered in solution. This conclusion is further supported by the corresponding ab initio calculated envelope and Kratky plot that displays a significant increase in $I \times q^2$ at higher q values (Figures S3B and S3C), characteristic of proteins containing disordered regions (Putnam et al., 2007).

HsCEP135-N 82–144 resulted in crystals with two monomers in the asymmetric unit. The monomers formed a two-stranded parallel and in register coiled-coil structure (Figure 3B), consistent with the CD analysis of HsCEP135-N 82–144 in solution at 4°C (Figure S2B). Knobs-into-holes packing was observed for heptad **a** and **d** core residues spanning segment ~80–130. Notably, Cys110 at a heptad **d** core position of HsCEP135-N 82–144 forms a disulfide bridge with Cys110′ from the neighboring chain (Figure 3B).

Next, we analyzed His-HsCEP135-N by SAXS (Figure 4C). As shown in Figure 4D, the corresponding calculated distance distribution function revealed a similarly distinct peak centered at 24 Å as obtained for CrBld10p-N 1–70, in agreement with the approximate thickness of a two-stranded coiled-coil structure. It further suggested the presence of a highly elongated molecule with a D_{max} of 213 Å (Table 3). In line with this conclusion, the corresponding Kratky plot and the ab initio calculated envelope indicate a predominantly elongated and folded protein (Figures S3D and S3E). However, the course of the Kratky plot in the high q range indicates the presence of some disorder; based on our data obtained CrBld10p-N 1–70, we attributed this disorder to the N-terminal residues of the protein. The molecular masses derived from the SAXS data using the Rambo-Tainer method (Rambo and Tainer, 2013) and from the volume of the molecular SAXS envelope amounts to 40 and 54 kDa, respectively, in good agreement with the calculated molecular mass for the His-HsCEP135-N dimer (40.6 kDa; Table 3).

In order to generate a full atomic model of HsCEP135-N, we performed homology modeling followed by molecular dynamics simulations using the crystal structures of CrBld10p-N 1–70 (42% and 53% sequence identity and similarity, respectively, to HsCEP135-N 1–70) and HsCEP135-N 82–144 as a basis (Figure 5A). Consistent with the SAXS data, the resulting HsCEP135-N model shows an extended homo-dimeric coiled-coil structure ~190 × ~25 Å in size (Figure 5B). The theoretical distance distribution function calculated from the model shows a similar peak and D_{max} as the distance distribution function derived from the His-HsCEP135-N SAXS data with a goodness of fit (χ) measure of 1.21 (Figures 5C and S3F). The fit is particularly good in the low q range that contains the general molecular shape information and deviates in the high q region that contains more detailed feature information (Putnam et al., 2007). Notably, the HsCEP135-N model shows a bend that is caused by a proline residue in the sequence (Pro70). A bend at the corresponding position is also observed in the ab initio envelope generated from the SAXS data (Figures 5B and 5D) and is supported by the fact that prolines can introduce kinks in coiled-coil structures (Chang et al., 1999). The overall conformation of the model fits well into the SAXS envelope and matches the observed SAXS scattering data obtained from His-HsCEP135-N (Figures 5C, 5D, and S3F). Further analysis of the HsCEP135-N atomic model revealed three patches along the coiled coil (denoted 1, 2, and 3), which display strikingly high positive electrostatic surface potentials (Figure 5E).

Collectively, our biophysical and structural data suggest that the predominantly positively charged N-terminal domain of HsCEP135 forms an extended two-stranded coiled-coil structure with chains arranged in parallel and in register. They further indicate that the first ~25–30 N-terminal residues of HsCEP135 are largely disordered in solution and adopt an ensemble of different conformations.

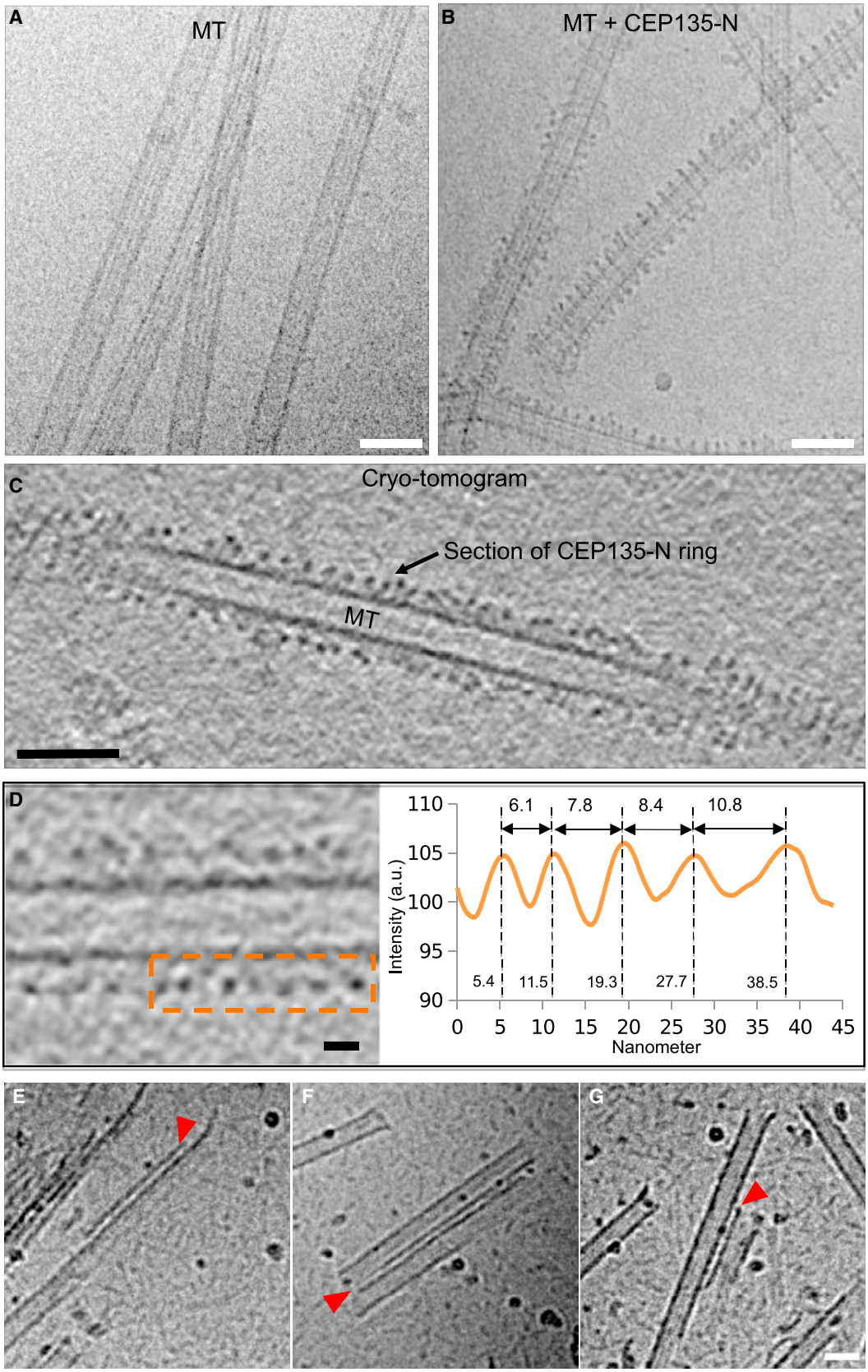

(legend on next page)

Table 2. X-Ray Data Collection, Phasing, and Refinement Statistics

	HsCEP135 82–144 PDB: 5FCN	CrBld10 1–70 PDB: 5FCM
Data Collection		
Space group	I41 22	I41 22
Cell dimensions		
a, *b*, *c* (Å)	78.85, 78.85, 95.92	92.74, 92.74, 164.07
α, β, γ	90, 90, 90	90, 90, 90
Wavelength	1.00	2.0664
Resolution (Å)	39.42–1.8 (1.864–1.8)	47.11–2.229 (2.309–2.229)
R_{merge}	0.04226 (0.4213)	0.1071 (2.16)
$I/\sigma I$	18.71 (3.49)	50.27 (1.11)
Completeness (%)	99.00 (99.0)	100.00 (97.00)
Redundancy	4.8 (5.0)	103.5 (14.9)
Refinement		
Resolution (Å)	39.42–1.8 (1.864–1.8)	47.11–2.229 (2.309–2.229)
No. of reflections	14,194 (1,393)	17,800 (1,694)
R_{work}/R_{free}	0.2169/0.2394 (0.3052/0.3524)	0.2142/0.2363 (0.4435/0.4213)
No. of atoms	1,058	2,150
Protein	913	2091
Ligand/ion	0	33
Water	145	26
B factors		
Protein	37.07	64.17
Ligand/ion		72.70
Water	36.90	56.34
RMSD		
Bond lengths (Å)	0.002	0.003
Bond angles (°)	0.37	0.56

Values in parentheses refer to the highest-resolution shell.

Identification and Characterization of a Microtubule-Binding Site in HsCEP135-N

We set out to narrow down the microtubule-binding region in HsCEP135-N. For this purpose, we generated several N- or C-terminal truncations and recombinantly expressed and purified the resulting fragments (Figure 1A). The structural integrity of the various fragments was assessed by CD and SEC-MALS. As shown in Figure S4 and summarized in Table 1, like the full-length HsCEP135-N domain, most of the fragments thereof formed dimeric coiled-coil structures. An exception was HsCEP135-N 96–158, which was monomeric in reducing buffer conditions; however, under non-reducing conditions, HsCEP135-N 96–158 formed a stable coiled-coil dimer. This result can be explained by the presence of a cysteine residue at a heptad **d** core position in HsCEP135-N (Cys110), which allows for the formation of a disulfide bridge in the context of a two-stranded parallel and in register coiled-coil structure (Chernyatina and Strelkov, 2012). This analysis shows that all HsCEP135-N fragments produced preserved the two-stranded coiled-coil structure of the full-length protein under appropriate buffer conditions.

Next, the microtubule-binding activities of the dimeric HsCEP135-N fragments were tested using microtubule pelleting assays. As summarized in Table 1 and shown in Figure 6A, the two minimal HsCEP135-N fragments 1–108 and 96–158 retained the ability to pellet together with microtubules. This observation suggests that a microtubule-binding site is located between residues 96 and 108. Notably, this segment coincides with the positively charged surface patch 2 identified in our atomic HsCEP135-N model (Figure 5E). It is well known that clusters of basic amino acids of microtubule-binding domains are frequently implicated in mediating interactions with the negatively charged outer surface of microtubules (Ciferri et al., 2008; Fourniol et al., 2010; Maurer et al., 2012). We thus tested the functional relevance of selected basic residues in this region. Inspection of the HsCEP135-N 82–144 crystal structure revealed three lysine residues, K101, K104, and K108, which are present in the microtubule-binding region 96–108 (Figures 6B and 6C) and which are responsible for the high positive electrostatic surface potential of patch 2 (Figures 5E and 6C). To test the relevance of these three lysine residues we simultaneously mutated them to alanine in HsCEP135-N 96–158 (HsCEP135-N 96–158 3xK), HsCEP135-N 68–158 (HsCEP135 68–158 3xK), HsCEP135-N 1–108 (HsCEP135 1–108 3xK), and HsCEP135-N (HsCEP135-N 3xK). Analysis by CD and SEC-MALS demonstrated that all four triple mutants maintained dimeric coiled-coil structures in solution (Figure S4 and Table 1; HsCEP135-N 96–158 3xK was assessed under non-reducing buffer conditions).

The microtubule-binding activities of the various HsCEP135-N mutants were assessed by microtubule pelleting assays. In contrast to wild-type, HsCEP135-N 96–158 3xK did not pellet together with microtubules (Figure 6A), suggesting that residues K101, K104, and K108 are important for microtubule binding of this HsCEP135-N fragment. HsCEP135-N 68–158 3xK and HsCEP135-N 1–108 3xK retained some microtubule-binding activity as indicated by the weaker bands in the corresponding pellet fractions (Figure 6A). Intriguingly, HsCEP135-N 3xK still pelleted together with microtubules, suggesting that this mutant retained the capacity to somehow interact with microtubules as tested in this assay (Figure 6A).

To investigate these observations further, we conducted immunofluorescence experiments of microtubules that were mixed with either HsCEP135-N 3xK or HsCEP135 96–158 3xK

Figure 2. Cryo-EM Analysis of Assemblies Formed between Microtubules and HsCEP135-N

(A and B) Cryo-EM micrograph showing decoration of Taxol-stabilized microtubules (MT) incubated without (A) and with (B) HsCEP135-N. Scale bars, 50 nm.
(C and D) Different cryo-EM tomograms of Taxol-stabilized MTs incubated with HsCEP135-N (D, left) and corresponding analysis of the intensity distribution along the outer microtubule edge (D, right, dashed rectangle). a.u., arbitrary units. Scale bars, 50 and 10 nm for (C) and (D), respectively.
(E–G) Cryo-EM micrographs of higher-order tubulin assemblies obtained by co-polymerizing tubulin and HsCEP135-N. Apparent are microtubules bridged with a protofilament (E) or with another microtubule (F and G, red arrowheads). Scale bar, 40 nm. See also Figure S1.

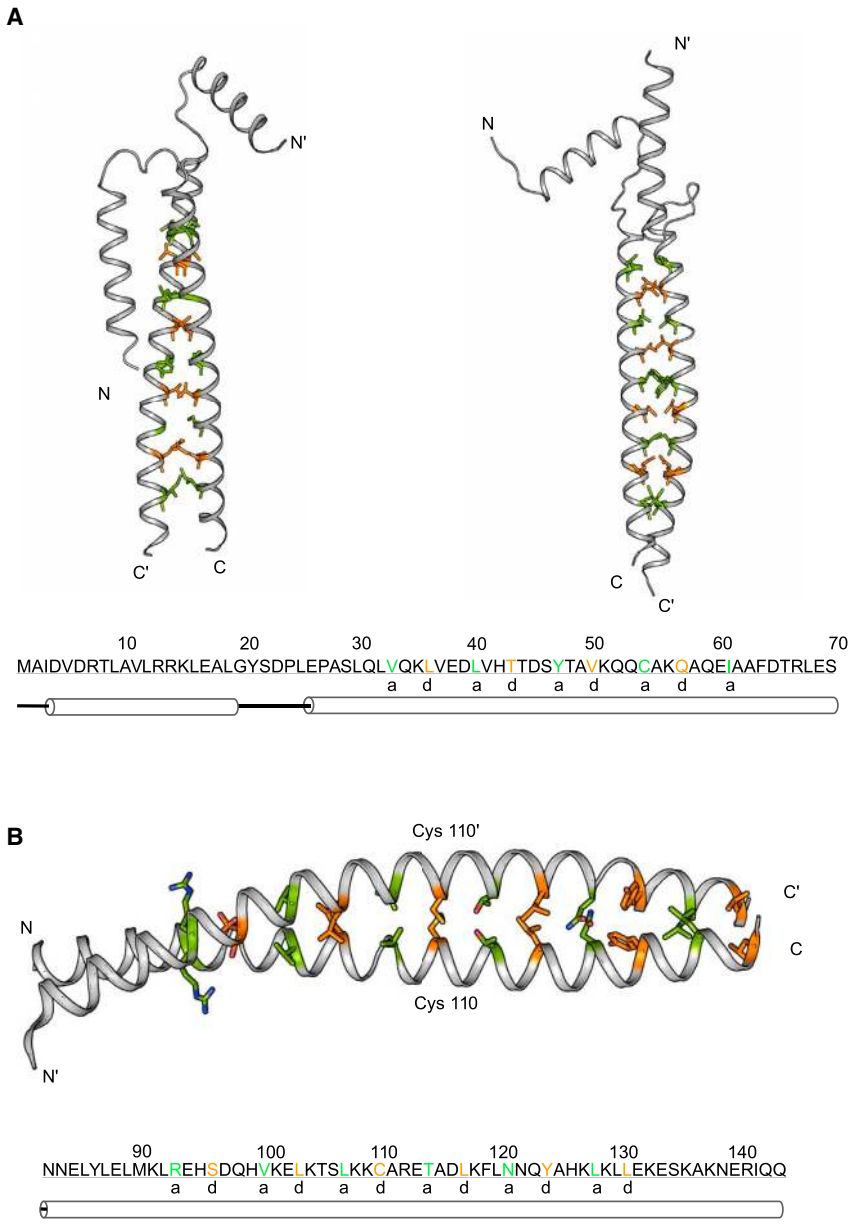

Figure 3. Crystal Structures of CrBld10p-N 1–70 and HsCEP135-N 82–144

(A) Crystal structures of the two CrBld10p-N 1–70 dimers found in the asymmetric unit of the crystal and aligned vertically for side-to-side comparison. (B) Crystal structures of the single HsCEP135-N 82–144 dimer present in the asymmetric unit of the crystal. The corresponding sequence and structure-based secondary structure assignments are shown below the structures. Residues occupying heptad **a** and **d** core positions that pack in a knobs-into-holes fashion are shown in green and orange sticks representation, respectively.
See also Figure S2.

(i.e., two mutants showing either binding or no binding in pelleting assays) or with their respective wild-type variants, before being spun onto coverslips and stained with antibodies against α-tubulin and HsCEP135-N. As shown in Figure 7A, microtubules did not significantly pellet on their own in this assay; however, in the presence of wild-type HsCEP135-N, crosslinked and bundled microtubules were present on the coverslip (Figure 7B). This effect is reminiscent of classical microtubule-stabilizing proteins (Lewis et al., 1989; Kanai et al., 1992) or of proteins that stabilize microtubules by inducing bundling upon overexpression (Hoogenraad et al., 2000; Bu and Su, 2003), suggesting that HsCEP135-N has a stabilizing effect on microtubules in vitro. By contrast, microtubules, while present, were much less crosslinked/bundled with one another in the presence of HsCEP135-N 3xK (Figure 7C). Similar experiments carried out with the HsCEP135-N 96–158 variant established that, whereas the wild-type fragment interacted with microtubules, no microtubules were spun onto the coverslip in the presence of HsCEP135-N 96–158 3xK (Figure 7D; note that the HsCEP135-N antibodies do not recognize the HsCEP135-N 96–158 fragment). These results are fully consistent with the ones obtained with the microtubule pelleting assay (Figure 6A) and concur to establish that residues K101, K104, and K108 are critical for efficient microtubule crosslinking/bundling by HsCEP135-N.

Collectively, these results narrow down a major microtubule-binding site in HsCEP135-N to a 13 amino acid region (segment 96–108). They further identify three surface-exposed lysine residues in this segment, which confer the microtubule crosslinking/bundling activity of the HsCEP135-N in vitro; however, they also indicate that additional elements flanking segment 96–108 contribute to the overall microtubule-binding affinity of HsCEP135-N. Based on our current mutagenesis data, we suspect that such elements are likely to be present on the N-terminal side of segment 96–108, since the mutant HsCEP135-N 96–158 3xK failed to interact with microtubules in pelleting assays. Thus, it is likely that the dimeric structure in combination with multiple microtubule-binding sites per monomer is the source of the microtubule crosslinking/bundling activity of HsCEP135-N.

Conclusions

There is a general agreement that CEP135/Bld10p promotes the assembly and stability of the centriolar microtubule wall and hence of the entire centriole organelle from algae to humans. However, in the absence of structural information prior to this work, how this protein family exerts this role at a mechanistic level has remained elusive. Here, by combining structural, biophysical, and biochemical approaches we have characterized in detail the structure of the N-terminal domain of human CEP135/Bld10p in vitro. We found that HsCEP135-N

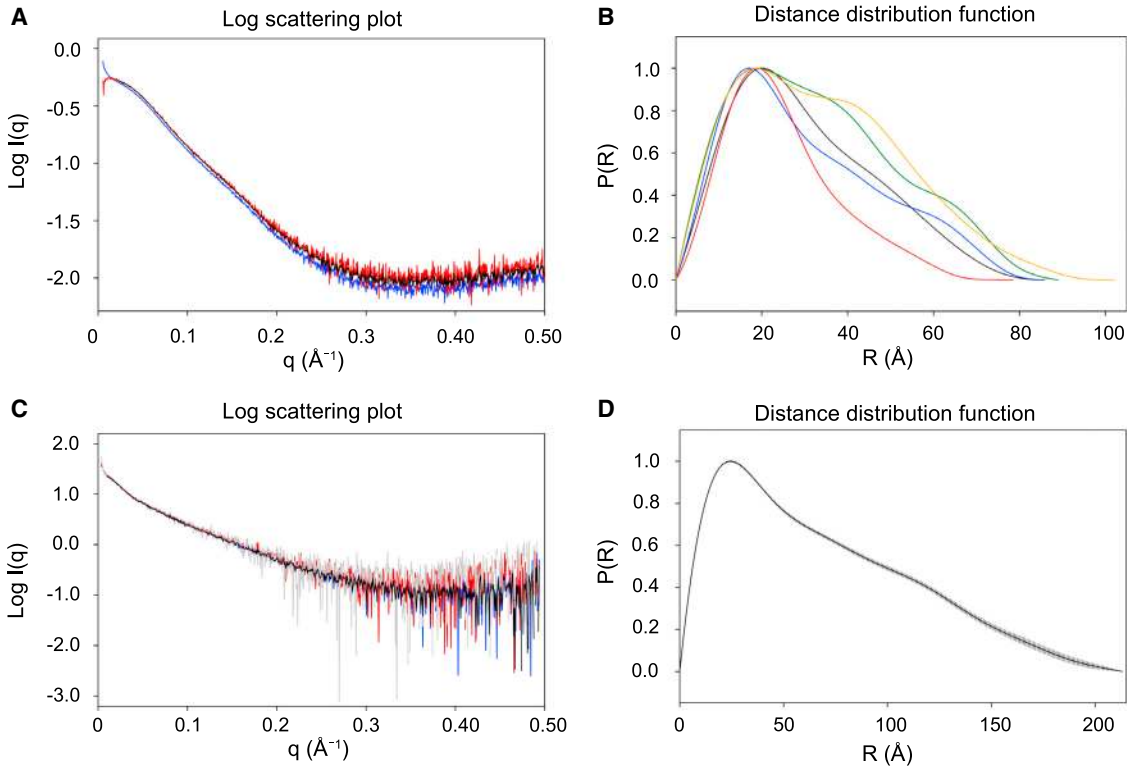

Figure 4. SAXS Analysis of CrBld10p-N 1–70 and HsCEP135-N

(A) Raw SAXS data of CrBld10p-N 1–70 recorded at a protein concentration of 2.5 (red profile) and 5 mg/ml (blue profile). The black profile corresponds to the merged data that were used for further processing.

(B) Distance distribution functions calculated from the experimental SAXS data (black profile) and from the four possible homo-dimeric CrBld10p-N 1–70 configurations (blue, red, green, and orange profiles) modeled from the four monomer structures present in the asymmetric unit of the crystal (Figure 3A).

(C) Raw SAXS data of His-HsCEP135-N recorded at 0.625 (gray profile), 1.25 (red profile), and 2.5 mg/ml (blue profile). The black profile corresponds to the merged data that were used for further processing.

(D) Distance distribution function calculated from the experimental SAXS data of His-HsCEP135-N. Error bars are depicted as gray vertical lines.

See also Figure S3.

forms a very stable, parallel, two-stranded coiled-coil structure. Our results further suggest that the ~30 N-terminal residues of HsCEP135-N are possibly disordered in solution. Interestingly, these residues belong to an ~40 amino acid stretch that is the most conserved region among the members of the CEP135/Bld10p family of proteins (Carvalho-Santos et al., 2010). The

Table 3. SAXS Data

Protein	Construct	Concentration (mg/ml)	R_G (Å)	D_{max} (Å)	Calculated MW (kDa)	Determined MW (kDa) by SAXS	Oligomerization State
HsCEP135	His-tagged 1–158	2.5	60.2	170–202	20.03	37.4[a]	dimer
HsCEP135	His-tagged 1–158	1.25	60.4	180–208	20.03	41.4[a]	dimer
HsCEP135	His-tagged 1–158	0.62	60.4	180–210	20.03	42.3[a]	dimer
HsCEP135	His-tagged 1–158	average			20.03	24.1[b]	
CrBld10	1–70	5	24.7	70–80	7.95	16.9[a]	dimer
CrBld10	1–70	2.5	24.1	75–85	7.95	17.1[a]	dimer
CrBld10	1–70	average			7.95	23.0[b]	

R_G, radius of gyration.

[a]Determined using the Rambo-Tainer method (Rambo and Tainer, 2013).

[b]Determined using BSA as a standard.

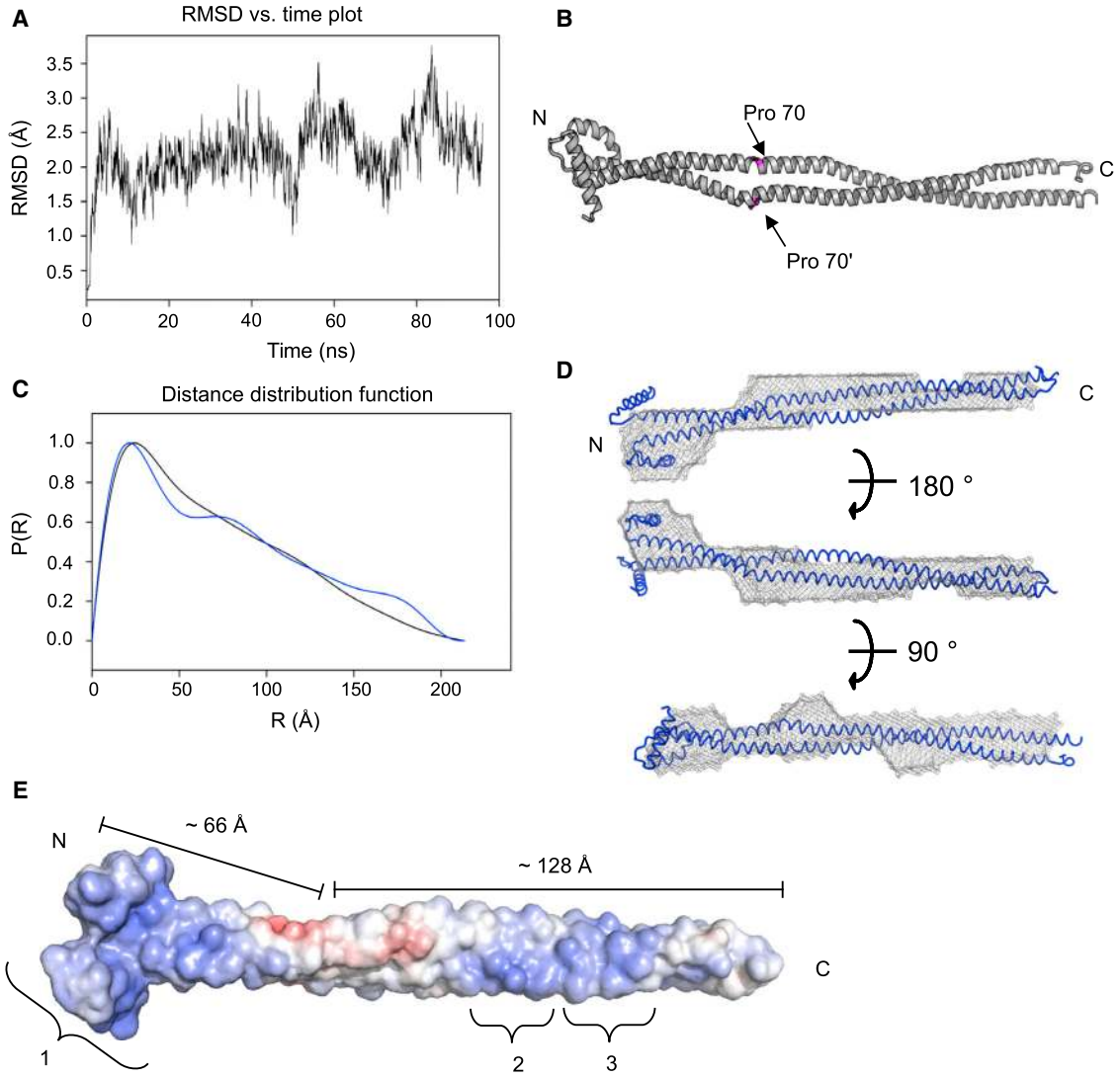

Figure 5. Atomic Model of HsCEP135-N

(A) Root-mean-square deviation (RMSD) of C_α atoms of HsCEP135-N over the molecular dynamics simulation trajectory. Only residues 82–133 were used for the calculation as the N and C terminus of HsCEP135-N are flexible.

(B) Simulated structure of HsCEP135-N with the Pro70 residue highlighted (magenta). Pro70 introduces a kink in the structure consistent with the ab initio SAXS envelope. A representative conformation from the largest cluster is shown.

(C) Distance distribution function calculated from the experimental SAXS data of His-HsCEP135-N (black profile) and from the atomic model of HsCEP135-N (blue profile) that was derived by modeling and molecular dynamics simulations.

(D) Overlay of the atomic model of HsCEP135-N from the modeling with the best His-HsCEP135-N DAMMIN envelope (Figure S3E).

(E) Surface view of the HsCEP135-N model, color-coded with the electrostatic surface potential calculated at pH 6.8 (from −10 to +10 k_BT; red and blue depict negative and positive electrostatic potentials, respectively). Regions of positive electrostatic potential are indicated and numbered with 1, 2, and 3.

See also Figure S3.

present data do not reveal the function of this most N-terminal segment; due to its high conservation across evolution, we expect that this part of CEP135/Bld10p may represent a binding site for centriolar protein partner(s) that awaits identification.

It has been recently reported that there is a short human CEP135/Bld10p splice isoform (dubbed CEP135mini) comprising the first 249 N-terminal residues of HsCEP135, plus 16 amino acids that differ in sequence from the full-length protein (Dahl et al., 2015). This shorter HsCEP135 variant negatively regulates centriole assembly by inhibiting the activity of the full-length protein, presumably by preventing it from interacting with centriolar binding partners such as HsSAS-6 (Dahl et al., 2015). Notably, our HsCEP135-N atomic model accounts for the first approximately two-thirds of CEP135mini. It is well established that coiled-coil proteins can readily exchange their chains (Lehrer et al., 1989). One possibility to explain the inhibitory effect of CEP135mini is thus that it forms heterodimers with HsCEP135 and in this way negatively regulates the activity of the full-length protein.

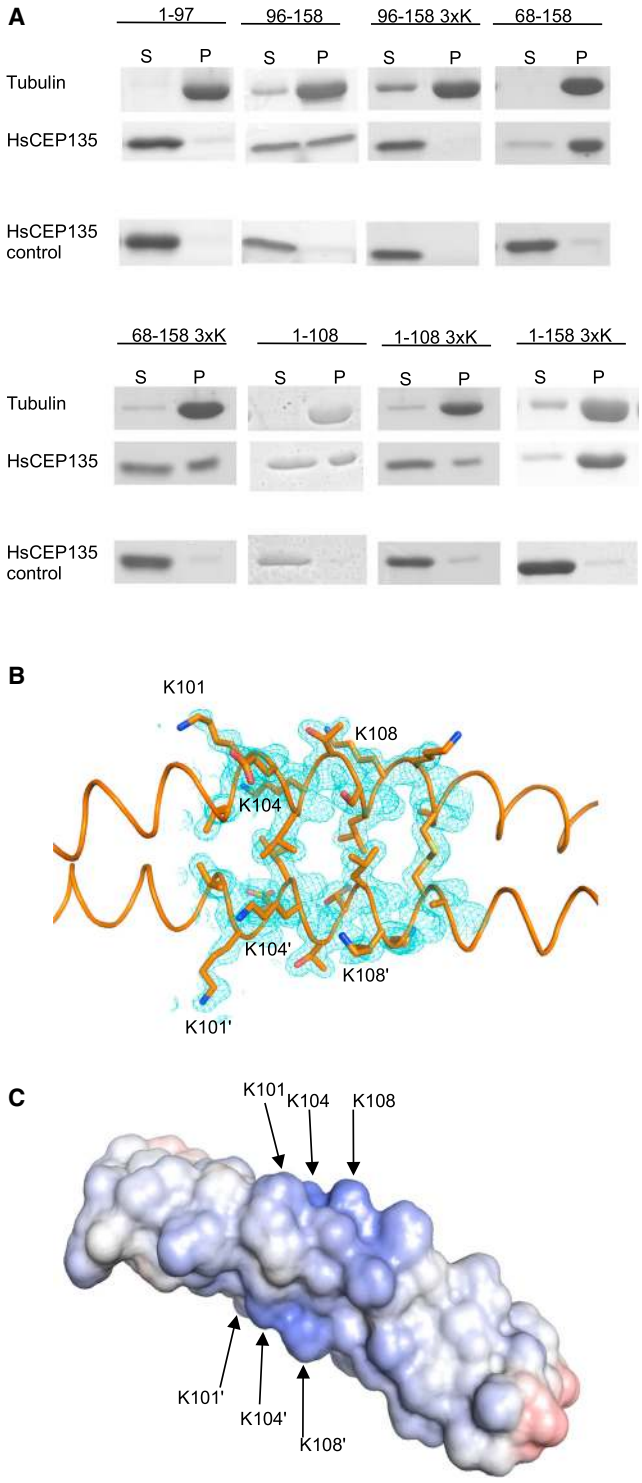

Figure 6. Identification of a Microtubule-Binding Site in HsCEP135-N

(A) Microtubule pelleting assays for the indicated HsCEP135-N fragments and mutants. Shown are relevant areas of Coomassie-stained SDS-PAGE gels.

(B) Close-up view of the microtubule-binding site in the crystal structure of HsCEP135-N 82–144 in cartoon representation. Residues K101, K104, and K108 that were simultaneously mutated are shown in sticks representation. The $2F_o - F_c$ electron density map (blue mesh) contoured at 1σ is superimposed onto the structure.

(C) Surface view of HsCEP135-N 82–144 color-coded with the electrostatic surface potential calculated at pH 6.8 (from −10 to +10 k_BT; red and blue depict negative and positive electrostatic potentials, respectively).

See also Figure S4.

Our study demonstrates that the N-terminal part of HsCEP135 binds tubulin, straight and curved protofilaments, and microtubules in vitro; to the best of our knowledge, this is the first demonstration that a coiled-coil domain can bind different types of tubulin assemblies. Our results further reveal that HsCEP135-N can crosslink/bundle and thus stabilize microtubules, which can be explained by the homo-dimeric structure of HsCEP135-N harboring multiple microtubule-binding sites. The capacity of HsCEP135-N to simultaneously bind two or more microtubules could contribute to the formation of microtubule triplets or else to linking neighboring triplets within the centriolar microtubule wall. In this context, it has been reported that HsCEP135 binds CPAP (Lin et al., 2013), an essential centriolar protein that interacts with tubulin and the γ-tubulin complex, and which is crucially involved in centriole biogenesis (Hung et al., 2000; Kohlmaier et al., 2009; Schmidt et al., 2009; Tang et al., 2009). A next goal will be to define how full-length HsCEP135 is spatially organized in the lumen of centrioles and how and to what extent its N-terminal domain collaborates with additional protein partners to control the assembly and stability of the centriolar microtubule wall.

EXPERIMENTAL PROCEDURES

Protein Preparation and Biophysical Characterization

Standard protein production in bacteria and peptide synthesis is described in the Supplemental Information. For CD spectroscopy, protein samples were diluted to a final concentration of 10 or 20 μM in PBS (pH 7.5), supplemented with 300 mM NaCl. For measurements under reducing conditions, 2 mM tris(2-carboxyethy1)phosphine or 2 mM DTT were added to the protein samples. Far-UV CD spectra recorded at 4°C and thermal unfolding profiles recorded at 222 nm were obtained on a Chirascan spectrophotometer (Applied Photophysics) equipped with a temperature control unit and sample temperature sensors. SEC-MALS experiments were performed in 20 mM Tris-HCl (pH 7.5), supplemented with 150 mM NaCl and 1 mM DTT using an S-200 10/30 analytical SEC column connected inline to miniDAWN TREOS light scattering and Optilab T-rEX refractive index detectors (Wyatt Technology).

Microtubule Pelleting Assay and Immunofluorescence Analysis

Standard microtubule pelleting assays were performed as previously described (Campbell and Slep, 2011). See also Supplemental Information. For immunofluorescence analysis, 10 μM Taxol-stabilized microtubules were mixed with an equimolar amount of HsCEP135-N variants and spun down on a coverslip for 10 min at 10,000 × *g*. Samples were then fixed in ice-cold methanol for 5 min followed by a wash in PBS and incubation with blocking solution (1%, w/v, BSA in PBS, 0.5% Tween 20 [PBT]) for 30 min. Primary and secondary antibodies were diluted in PBT as follows: mouse anti-α-tubulin (clone DM1A; Sigma-Aldrich): 1/1,000; rabbit anti-HsCEP135 1–158 (Meritxell Orpinell and P.G., unpublished data): 1/500; goat anti-rabbit Alexa Fluor 488 and goat anti-mouse Alexa Fluor 568 (both Life Technologies): both 1/1,000. Primary antibodies were incubated at 4°C overnight and secondary antibodies at room temperature for 1 hr, and the slides were washed with PBT. All images were processed with ImageJ (Schneider et al., 2012).

Electron Microscopy

Specimens were prepared by incubating Taxol-stabilized microtubules (20 μl of 10 μM tubulin in BRB80, prepared similarly as for the microtubule pelleting assay) with an equimolar amount of HsCEP135-N variants. Then, 2 μl of a 100 μM solution of soluble tubulin was added to the mix after 5 min of

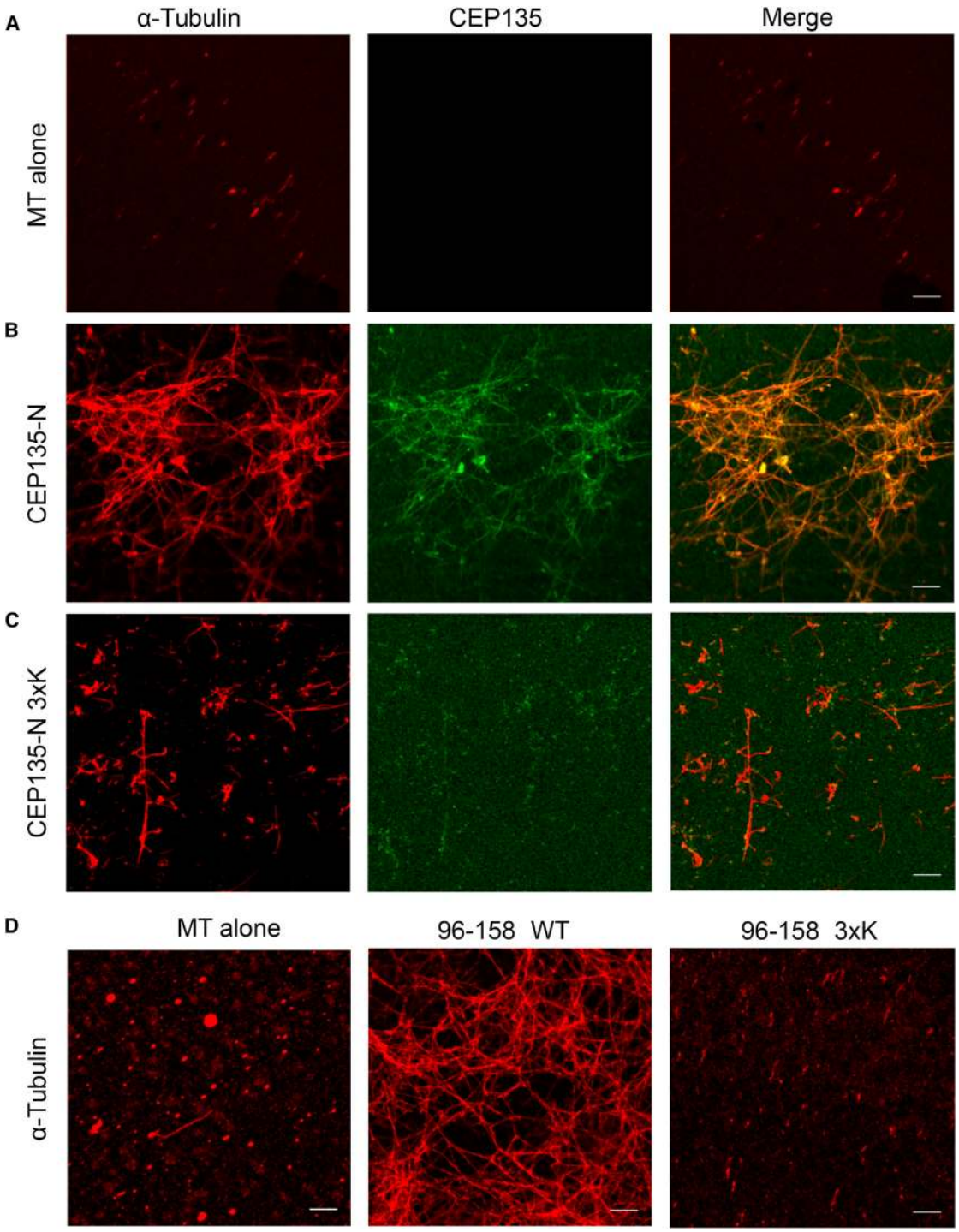

Figure 7. Immunofluorescence Microscopy of Microtubules in the Absence and Presence of HsCEP135-N Variants

(A–D) Fluorescence images of microtubules pelleted alone or in the presence of indicated wild-type or mutant HsCEP135-N variants and revealed by immunofluorescence microscopy with α-tubulin and HsCEP135 antibodies. Scale bars, 5 μm. Note that the HsCEP135-N antibodies do not recognize epitopes in the 96–158 region and are thus not shown in (D).

incubation to prevent formation of microtubule bundles. Tubulin ring-like oligomers were formed by mixing 10 μl of 100 μM soluble tubulin with equimolar amounts of HsCEP135-N 68–158. Bridged microtubules were obtained by mixing and incubation of an equimolar amount of free tubulin with HsCEP135 68–158 for 30 min followed by addition of 0.2 mM Taxol final concentration and further incubation for 1 hr at 37°C. Protein samples were adsorbed onto Lacey carbon film grids (300 microMesh), blotted with a filter paper (Whatman) and vitrified in liquid ethane using a homemade plunging apparatus. Samples were imaged with an FEG Tecnai F 20 (FEI) transmission electron microscope operated at 200 kV. For additional details, see Supplemental Information.

Crystallization, X-Ray Data Collection, and Structure Solution

Standard crystallization and X-ray data collection is described in the Supplemental Information. All datasets were reduced, scaled, and merged using XDS, XSCALE, and XDSCONV (Kabsch, 2010a, 2010b). For CrBld10p 1–70, phases were obtained by sulfur SAD phasing using SHELX via the HKL2MAP interface (Pape and Schneider, 2004; Thorn and Sheldrick, 2013). Automatic model building was done with BUCCANEER (Cowtan, 2012). Refinement was performed by alternating rounds of model building using the model building program COOT (Emsley et al., 2010) and refinement with Phenix.refine from the PHENIX suite (Adams et al., 2010).

For HsCEP135-N 82–144, the phase problem was solved by molecular replacement using the coiled-coil structure of GCN4 (PDB: 4GKW) as a search model. After obtaining an initial PHASER (McCoy et al., 2007) solution, the model was first improved manually based on the electron density using COOT (Emsley et al., 2010), then chain traced with SHELXE (Thorn and Sheldrick, 2013) and built with BUCCANEER (Cowtan, 2012). Refinement was performed as for CrBld10p 1–70. See Table 2 for all data collection and refinement statistics.

SAXS Measurements

SAXS measurements were performed at the cSAXS (X12SA) beamline at the Swiss Light Source (Paul Scherrer Institut) and at the BM29 bio-SAXS beamline at the European Synchrotron Radiation Facility (Pernot et al., 2013) at 10°C and 20°C, respectively. All measurements were taken at 1 Å wavelength. The q value is defined as $4\pi \times \sin\theta/\lambda$, where 2θ is the scattering angle.

Prior to the measurements, all samples were either spun down or filtered to remove possible aggregates. Concentrations ranging from 0.3 to 10 mg/ml for His-HsCEP135-N and from 1.25 to 5 mg/ml for CrBld10p 1–70 were measured. Data were analyzed in parallel using the ATSAS software suite (Petoukhov et al., 2012) and using an in house software package. Merging and cutting of the data was performed with PRIMUS (Konarev et al., 2003). The distance distribution functions were calculated using GNOM (Svergun, 1992) and were used as input for the DAMMIF/DAMMIN ab initio shape reconstruction (Franke and Svergun, 2009). Calculated distance distribution functions were generated with GNOM from simulated scattering data that were computed from atomic models with CRYSOL (Svergun et al., 1995).

Molecular Modeling and Molecular Dynamics Simulation

An atomic model of the HsCEP135-N was built using Modeller 9v14 (Webb and Sali, 2014) using our crystal structures of CrBld10p-N 1–70 and HsCEP135-N 82–144. Missing residues 71–81 and 145–158 were modeled in an α-helical configuration by introducing restraints on symmetry and secondary structure, as the protein forms a homo-dimeric coiled-coil structure. A set of 50 models were generated and evaluated using the discrete optimized protein energy (DOPE) values. The model with the best DOPE value was then further energy minimized and subjected to molecular dynamics simulations.

The model was first solvated in water and the charge of the system was then neutralized by adding 12 Cl^- ions. The final system comprised 450,890 atoms (1 HsCEP135-N, 148,246 waters, and 418 K^+ and 430 Cl^- ions). The complete system was first equilibrated at 310 K and 1 atm pressure for 24 ns and simulated for an additional 72 ns. All the simulations were performed using the CHARMM force field (Mackerell, 2004) in the NAMD2.10 package (Phillips et al., 2005). Trajectories were visualized using VMD (Humphrey et al., 1996) and clustering based on root-mean-square deviation was performed. A representative conformation from the largest cluster was used for figure preparation and comparison with the SAXS data. The theoretical scattering curve of the generated model was computed and compared using the program CRYSOL (Svergun et al., 1995) using the default parameters. The model was aligned with the SAXS envelope of HsCEP135-N 1–158 via SUPCOMB (Kozin and Svergun, 2001).

ACCESSION NUMBERS

Coordinates have been deposited at the PDB under the following accession numbers: HsCEP135-N 82–144 (PDB: 5FCN) and Bld10p-N 1–70 (PDB: 5FCM).

SUPPLEMENTAL INFORMATION

Supplemental Information includes Supplemental Experimental Procedures and four figures and can be found with this article online at http://dx.doi.org/10.1016/j.str.2016.06.011.

AUTHOR CONTRIBUTIONS

S.K., P. Guichard, J.M.O., N.O., G.N.H., M.H., I.S., J.M., P. Gönczy, and M.O.S. designed the experiments. S.K., P. Guichard, J.M.O., N.O., G.N.H., M.H., I.S., and J.M. conducted the experiments. S.K. and M.O.S. wrote the manuscript with input from all authors.

ACKNOWLEDGMENTS

We are grateful to Andreas Menzel, Vincent Olieric, and Meitian Wang for excellent technical assistance at the beamlines, to Richard Kammerer for the help with protein production, to Samin Akbari for assistance with the SAXS data collection, to Edward Lowe for acquiring SAXS data at the ESRF, and to Takashi Ishikawa for support. We also thank the Swiss National Supercomputing Centre (CSCS) for providing the necessary infrastructure for performing computational modeling and simulations. This work was supported by grants from the NCCBI (to J.M.O), the ERC (AdG 233335 and AdG 340227; to P.G.) and the Swiss National Science Foundation (310030B_138659; to M.O.S.).

Received: January 13, 2016
Revised: June 7, 2016
Accepted: June 10, 2016
Published: July 28, 2016

REFERENCES

Adams, P.D., Afonine, P.V., Bunkóczi, G., Chen, V.B., Davis, I.W., Echols, N., Headd, J.J., Hung, L.-W., Kapral, G.J., Grosse-Kunstleve, R.W., et al. (2010). PHENIX: a comprehensive Python-based system for macromolecular structure solution. Acta Crystallogr. D. Biol. Crystallogr. *66*, 213–221.

Azimzadeh, J., and Marshall, W. (2010). Building the centriole. Curr. Biol. *20*, R816–R825.

Bayless, B.A., Giddings, T.H., Winey, M., and Pearson, C.G. (2012). Bld10/Cep135 stabilizes basal bodies to resist cilia-generated forces. Mol. Biol. Cell *23*, 4820–4832.

Bettencourt-Dias, M., and Hildebrandt, F. (2011). Centrosomes and cilia in human disease. Trends Genet. *27*, 307–315.

Bornens, M. (2012). The centrosome in cells and organisms. Science *335*, 422–426.

Bu, W., and Su, L.-K. (2003). Characterization of functional domains of human EB1 family proteins. J. Biol. Chem. *278*, 49721–49731.

Campbell, J.N., and Slep, K.C. (2011). $\alpha\beta$-Tubulin and microtubule-binding assays. Methods Mol. Biol. *777*, 87–97.

Carvalho-Santos, Z., Machado, P., Branco, P., Tavares-Cadete, F., Rodrigues-Martins, A., Pereira-Leal, J.B., and Bettencourt-Dias, M. (2010). Stepwise evolution of the centriole-assembly pathway. J. Cell Sci. *123*, 1414–1426.

Carvalho-Santos, Z., Machado, P., Alvarez-Martins, I., Gouveia, S.M., Jana, S.C., Duarte, P., Amado, T., Branco, P., Freitas, M.C., Silva, S.T.N., et al. (2012). BLD10/CEP135 is a microtubule-associated protein that controls the formation of the flagellum central microtubule pair. Dev. Cell *23*, 412–424.

Chang, D.K., Cheng, S.F., Trivedi, V.D., and Lin, K.L. (1999). Proline affects oligomerization of a coiled coil by inducing a kink in a long helix. J. Struct. Biol. *128*, 270–279.

Chernyatina, A.A., and Strelkov, S.V. (2012). Stabilization of vimentin coil2 fragment via an engineered disulfide. J. Struct. Biol. *177*, 46–53.

Ciferri, C., Pasqualato, S., Screpanti, E., Varetti, G., Santaguida, S., Dos Reis, G., Maiolica, A., Polka, J., De Luca, J.G., De Wulf, P., et al. (2008). Implications for kinetochore-microtubule attachment from the structure of an engineered Ndc80 complex. Cell *133*, 427–439.

Cowtan, K. (2012). Completion of autobuilt protein models using a database of protein fragments. Acta Crystallogr. D. Biol. Crystallogr. *68*, 328–335.

Dahl, K.D., Sankaran, D.G., Bayless, B.A., Pinter, M.E., Galati, D.F., Heasley, L.R., Giddings, T.H., and Pearson, C.G. (2015). A short CEP135 splice isoform controls centriole duplication. Curr. Biol. *25*, 2591–2596.

Desai, A., Verma, S., Mitchison, T.J., and Walczak, C.E. (1999). Kin I kinesins are microtubule-destabilizing enzymes. Cell *96*, 69–78.

Emsley, P., Lohkamp, B., Scott, W.G., and Cowtan, K. (2010). Features and development of Coot. Acta Crystallogr. D. Biol. Crystallogr. *66*, 486–501.

Fourniol, F.J., Sindelar, C.V., Amigues, B., Clare, D.K., Thomas, G., Perderiset, M., Francis, F., Houdusse, A., and Moores, C.A. (2010). Template-free 13-protofilament microtubule-MAP assembly visualized at 8 A resolution. J. Cell Biol. *191*, 463–470.

Franke, D., and Svergun, D.I. (2009). DAMMIF, a program for rapid ab-initio shape determination in small-angle scattering. J. Appl. Crystallogr. *42*, 342–346.

Gönczy, P. (2012). Towards a molecular architecture of centriole assembly. Nat. Rev. Mol. Cell Biol. *13*, 425–435.

Guichard, P., Hachet, V., Majubu, N., Neves, A., Demurtas, D., Olieric, N., Fluckiger, I., Yamada, A., Kihara, K., Nishida, Y., et al. (2013). Native architecture of the centriole proximal region reveals features underlying its 9-fold radial symmetry. Curr. Biol. *23*, 1620–1628.

Hiraki, M., Nakazawa, Y., Kamiya, R., and Hirono, M. (2007). Bld10p constitutes the cartwheel-spoke tip and stabilizes the 9-fold symmetry of the centriole. Curr. Biol. *17*, 1778–1783.

Hirono, M. (2014). Cartwheel assembly. Philos. Trans. R. Soc. Lond. B. Biol. Sci. *369*, pii: 20130458.

Hoogenraad, C.C., Akhmanova, A., Grosveld, F., De Zeeuw, C.I., and Galjart, N. (2000). Functional analysis of CLIP-115 and its binding to microtubules. J. Cell Sci. *113*, 2285–2297.

Humphrey, W., Dalke, A., and Schulten, K. (1996). VMD: visual molecular dynamics. J. Mol. Graph. *14*, 33–38, 27–28.

Hung, L.Y., Tang, C.J., and Tang, T.K. (2000). Protein 4.1 R-135 interacts with a novel centrosomal protein (CPAP) which is associated with the gamma-tubulin complex. Mol. Cell. Biol. *20*, 7813–7825.

Hussain, M.S., Baig, S.M., Neumann, S., Nu, G., Farooq, M., Ahmad, I., Alef, T., Hennies, H.C., Technau, M., Frommolt, P., et al. (2012). A truncating mutation of CEP135 causes primary microcephaly and disturbed centrosomal function. Am. J. Hum. Genet. *90*, 871–878.

Jerka-Dziadosz, M., Gogendeau, D., Klotz, C., Cohen, J., Beisson, J., and Koll, F. (2010). Basal body duplication in Paramecium: the key role of Bld10 in assembly and stability of the cartwheel. Cytoskeleton (Hoboken) *67*, 161–171.

Kabsch, W. (2010a). Xds. Acta Crystallogr. D. Biol. Crystallogr. *66*, 125–132.

Kabsch, W. (2010b). Integration, scaling, space-group assignment and post-refinement. Acta Crystallogr. D. Biol. Crystallogr. *66*, 133–144.

Kanai, Y., Chen, J., and Hirokawa, N. (1992). Microtubule bundling by tau proteins in vivo: analysis of functional domains. EMBO J. *11*, 3953–3961.

Kitagawa, D., Vakonakis, I., Olieric, N., Hilbert, M., Keller, D., Olieric, V., Bortfeld, M., Erat, M.C., Flückiger, I., Gönczy, P., et al. (2011). Structural basis of the 9-fold symmetry of centrioles. Cell *144*, 364–375.

Kleylein-Sohn, J., Westendorf, J., Le Clech, M., Habedanck, R., Stierhof, Y.-D., and Nigg, E.A. (2007). Plk4-induced centriole biogenesis in human cells. Dev. Cell *13*, 190–202.

Kohlmaier, G., Lončarek, J., Meng, X., McEwen, B.F., Mogensen, M.M., Spektor, A., Dynlacht, B.D., Khodjakov, A., and Gönczy, P. (2009). Overly long centrioles and defective cell division upon excess of the SAS-4-related protein CPAP. Curr. Biol. *19*, 1012–1018.

Konarev, P.V., Volkov, V.V., Sokolova, A.V., Koch, M.H.J., and Svergun, D.I. (2003). PRIMUS: a windows PC-based system for small-angle scattering data analysis. J. Appl. Crystallogr. *36*, 1277–1282.

Kozin, M.B., and Svergun, D.I. (2001). Automated matching of high- and low-resolution structural models. J. Appl. Crystallogr. *34*, 33–41.

Lalor, P., Dockery, P., Kuriyama, R., Gergely, F., and Morrison, C.G. (2013). Abnormal centrosomal structure and duplication in Cep135-deficient vertebrate cells. Mol. Biol. Cell *24*, 2645–2654.

Lehrer, S.S., Qian, Y.D., and Hvidt, S. (1989). Assembly of the native heterodimer of Rana esculenta tropomyosin by chain exchange. Science *246*, 926–928.

Lewis, S.A., Ivanov, I.E., Lee, G.H., and Cowan, N.J. (1989). Organization of microtubules in dendrites and axons is determined by a short hydrophobic zipper in microtubule-associated proteins MAP2 and tau. Nature *342*, 498–505.

Lin, Y., Chang, C., Hsu, W., Tang, C.C., Lin, Y., Chou, E., Wu, C., and Tang, T.K. (2013). Human microcephaly protein CEP135 binds to hSAS-6 and CPAP, and is required for centriole assembly. EMBO J. *32*, 1141–1154.

Mackerell, A.D. (2004). Empirical force fields for biological macromolecules: overview and issues. J. Comput. Chem. *25*, 1584–1604.

Mandelkow, E.M., Mandelkow, E., and Milligan, R.A. (1991). Microtubule dynamics and microtubule caps: a time-resolved cryo-electron microscopy study. J. Cell Biol. *114*, 977–991.

Matsuura, K., Lefebvre, P.A., Kamiya, R., and Hirono, M. (2004). Bld10p, a novel protein essential for basal body assembly in Chlamydomonas: localization to the cartwheel, the first ninefold symmetrical structure appearing during assembly. J. Cell Biol. *165*, 663–671.

Maurer, S.P., Fourniol, F.J., Bohner, G., Moores, C.A., and Surrey, T. (2012). EBs recognize a nucleotide-dependent structural cap at growing microtubule ends. Cell *149*, 371–382.

McCoy, A.J., Grosse-Kunstleve, R.W., Adams, P.D., Winn, M.D., Storoni, L.C., and Read, R.J. (2007). Phaser crystallographic software. J. Appl. Crystallogr. *40*, 658–674.

Mottier-pavie, V., and Megraw, T.L. (2009). Drosophila Bld10 is a centriolar protein that regulates centriole, basal body, and motile cilium assembly. Mol. Biol. Cell *20*, 2605–2614.

Nigg, E.A., and Raff, J.W. (2009). Centrioles, centrosomes, and cilia in health and disease. Cell *139*, 663–678.

Ohta, T., Essner, R., Ryu, J.-H., Palazzo, R.E., Uetake, Y., and Kuriyama, R. (2002). Characterization of Cep135, a novel coiled-coil centrosomal protein involved in microtubule organization in mammalian cells. J. Cell Biol. *156*, 87–99.

Pape, T., and Schneider, T.R. (2004). HKL2MAP: a graphical user interface for macromolecular phasing with SHELX programs. J. Appl. Crystallogr. *37*, 843–844.

Pernot, P., Round, A., Barrett, R., De Maria Antolinos, A., Gobbo, A., Gordon, E., Huet, J., Kieffer, J., Lentini, M., Mattenet, M., et al. (2013). Upgraded ESRF BM29 beamline for SAXS on macromolecules in solution. J. Synchrotron Radiat. *20*, 660–664.

Petoukhov, M.V., Franke, D., Shkumatov, A.V., Tria, G., Kikhney, A.G., Gajda, M., Gorba, C., Mertens, H.D.T., Konarev, P.V., and Svergun, D.I. (2012). New developments in the ATSAS program package for small-angle scattering data analysis. J. Appl. Crystallogr. *45*, 342–350.

Phillips, J.C., Braun, R., Wang, W., Gumbart, J., Tajkhorshid, E., Villa, E., Chipot, C., Skeel, R.D., Kalé, L., and Schulten, K. (2005). Scalable molecular dynamics with NAMD. J. Comput. Chem. *26*, 1781–1802.

Putnam, C.D., Hammel, M., Hura, G.L., and Tainer, J.A. (2007). X-ray solution scattering (SAXS) combined with crystallography and computation: defining accurate macromolecular structures, conformations and assemblies in solution. Q. Rev. Biophys. *40*, 191–285.

Rambo, R.P., and Tainer, J.A. (2013). Accurate assessment of mass, models and resolution by small-angle scattering. Nature *496*, 477–481.

Roque, H., Wainman, A., and Richens, J. (2012). Drosophila Cep135/Bld10 maintains proper centriole structure but is dispensable for cartwheel formation. J. Cell Sci. *125*, 5881–5886.

Ryu, J.H., Essner, R., Ohta, T., and Kuriyama, R. (2000). Filamentous polymers induced by overexpression of a novel centrosomal protein, Cep135. Microsc. Res. Tech. *49*, 478–486.

Schmidt, T.I., Kleylein-Sohn, J., Westendorf, J., Le Clech, M., Lavoie, S.B., Stierhof, Y.-D., and Nigg, E.A. (2009). Control of centriole length by CPAP and CP110. Curr. Biol. *19*, 1005–1011.

Schneider, C.A., Rasband, W.S., and Eliceiri, K.W. (2012). NIH image to ImageJ: 25 years of image analysis. Nat. Methods *9*, 671–675.

Singh, P., Ramdas Nair, A., and Cabernard, C. (2014). The centriolar protein Bld10/Cep135 is required to establish centrosome asymmetry in Drosophila neuroblasts. Curr. Biol. *24*, 1548–1555.

Sonnen, K.F., Schermelleh, L., Leonhardt, H., and Nigg, E.A. (2012). 3D-structured illumination microscopy provides novel insight into architecture of human centrosomes. Biol. Open *1*, 965–976.

Svergun, D.I. (1992). Determination of the regularization parameter in indirect-transform methods using perceptual criteria. J. Appl. Crystallogr. *25*, 495–503.

Svergun, D., Barberato, C., and Koch, M.H.J. (1995). CRYSOL – a program to evaluate X-ray solution scattering of biological macromolecules from atomic coordinates. J. Appl. Crystallogr. *28*, 768–773.

Tan, D., Asenjo, A.B., Mennella, V., Sharp, D.J., and Sosa, H. (2006). Kinesin-13s form rings around microtubules. J. Cell Biol. *175*, 25–31.

Tang, C.-J.C., Fu, R.-H., Wu, K.-S., Hsu, W.-B., and Tang, T.K. (2009). CPAP is a cell-cycle regulated protein that controls centriole length. Nat. Cell Biol. *11*, 825–831.

Thorn, A., and Sheldrick, G.M. (2013). Extending molecular-replacement solutions with SHELXE. Acta Crystallogr. D. Biol. Crystallogr. *69*, 2251–2256.

Van Breugel, M., Hirono, M., Andreeva, A., Yanagisawa, H., Yamaguchi, S., Nakazawa, Y., Morgner, N., Petrovich, M., Ebong, I.-O., Robinson, C.V., et al. (2011). Structures of SAS-6 suggest its organization in centrioles. Science *331*, 1196–1199.

Walshaw, J., and Woolfson, D.N. (2001). Socket: a program for identifying and analysing coiled-coil motifs within protein structures. J. Mol. Biol. *307*, 1427–1450.

Wang, Q., Crevenna, A.H., Kunze, I., and Mizuno, N. (2014). Structural basis for the extended CAP-Gly domains of p150(glued) binding to microtubules and the implication for tubulin dynamics. Proc. Natl. Acad. Sci. USA *111*, 11347–11352.

Webb, B., and Sali, A. (2014). Comparative protein structure modeling using MODELLER. Curr. Protoc. Bioinformatics *47*, 5.6.1–5.6.32.

Zhou, N.E., Kay, C.M., and Hodges, R.S. (1992). Synthetic model proteins: the relative contribution of leucine residues at the nonequivalent positions of the 3-4 hydrophobic repeat to the stability of the two-stranded alpha-helical coiled-coil. Biochemistry *31*, 5739–5746.